

Noise Level and Blind Quality Evaluations in Abdominopelvic Electromagnetic X-ray Computed Tomographic Images using Deep-learning Reconstruction Method

Jina Shim¹, Seungwan Lee^{2*}, and Youngjin Lee^{3*}

¹Department of Diagnostic Radiology, Severance Hospital, 50-1, Yonsei-ro, Seodaemun-gu, Seoul, Republic of Korea

²Department of Radiological Science, Konyang University, 158, Gwanjeodong-ro, Seo-gu, Daejeon, Republic of Korea

³Department of Radiological Science, Gachon University, 191, Hambakmoero, Yeonsu-gu, Incheon, Republic of Korea

(Received 23 December 2023, Received in final form 10 March 2024, Accepted 18 March 2024)

This study aimed to confirm the characteristics of deep-learning image reconstruction (DLIR) intensity in abdominopelvic computed tomography (CT) using noise level and blind quality evaluation parameters. The study was conducted using phantoms and patients, and CT images were obtained while adjusting the intensity of DLIR to low (DLIR-L), middle (DLIR-M), and high (DLIR-H). To quantitatively evaluate image quality, the coefficient of variation (COV) and contrast-to-noise ratio (CNR), as well as natural image quality evaluation (NIQE) and blind/referenceless image spatial quality evaluator (BRISQUE), were used. In both the noise level and blind quality evaluation results, a higher strength of DLIR resulted in better results derived from the phantom and patient studies. In particular, the results of the phantom study confirmed that NIQE and BRISQUE of CT images acquired using DLIR-H were improved by approximately 5 % and 1 %, respectively, compared to the corresponding the application of DLIR-L. Moreover, when high-strength deep-learning was applied to a real patient's CT image reconstruction method, the NIQE and BRISQUE results improved by approximately 6 % and 4 %, respectively, compared with their respective medium levels. In conclusion, we quantitatively analyzed the image quality according to the intensity of the recently developed deep-learning-based CT image reconstruction method.

Keywords : Abdominopelvic computed tomography (CT), Deep-learning image reconstruction (DLIR) intensity, Noise level evaluation, Blind image quality evaluation

1. Introduction

The most used method for reconstructing cross-sectional images in computed tomography (CT) is filtered back-projection (FBP). This method is based on the principle of back-projecting X-ray projection data from various angles after filter correction. In this case, blurring of the reconstructed cross-sectional image can be removed using filter correction. The noise of the cross-section images can be removed according to the type of filter, and the spatial resolution may be improved. However, because FBP images require hundreds of projection images to obtain high-quality images and cause increased radiation exposure, the proposed method for obtaining high-quality images while lowering the radiation dose is an iterative

reconstruction (IR) [1].

IR consists of hybrid IR and model-based IR (MBIR). Hybrid IR has the advantages of fast reconstruction speed, high spatial resolution, and reduced exposure dose [2-5]. Adaptive statistical reconstruction (ASIR; GE Healthcare, Waukesha, Wisconsin, USA) is the most widely studied hybrid IR, which reduces radiation doses by 40 % while providing clinically acceptable image quality [6]. ASIR-V, which was developed by GE Healthcare, enables a feasible dose reduction while providing a better image quality than that provided by ASIR [7-9]. MBIR, which has become available as a fully iterative method, provides the flexibility to incorporate a model of each factor, such as X-ray tube response, detector response, system noise, object, photon statistics, and electronic noise [10,11]. It provides better image quality than FBP and ASIR, even at ultralow doses [1, 12]. However, some studies have reported that hybrid IR, especially when using IR of strong intensity, is related to image quality problems (e.g., an artificial texture or a blotchy ap-

©The Korean Magnetism Society. All rights reserved.

*Co-corresponding author: Tel:+82-42-600-8443,

e-mail: slee1@konyang.ac.kr (Seungwan Lee)

Tel:+82-32-820-4362, e-mail: yj20@gachon.ac.kr (Youngjin Lee)

pearance) [13, 14]. Additionally, MBIR requires a long processing time; thus, it is not widely used in clinical practice [1, 12, 15].

Recently, artificial intelligence technology has been developed by for application in CT image development [16]. Deep-learning image reconstruction (DLIR) outputs images by inputting sinogram data through a deep convolutional neural network that pre-trains large volumes of image data. The output images are obtained by mathematically comparing and analyzing “ground truth” images with the high-contrast resolution, low-contrast resolution, image noise, image texture, CT number accuracy, and anatomical characteristics. DLIR is expected to solve limitations of natural FBP images such as the unnatural texture in IR images [17].

For medical images, it is important to accurately visualize the information. However, a stronger intensity of reconstruction makes it difficult to determine whether all information has been visualized. In some IR studies, stronger intensity was associated with stronger artificial textures [14], which was not selected for clinical application. The intensity of DLIR has three stages. It is important to accurately determine and implement the amount of noise reduction and contrast enhancement based on the intensity of DLIR in clinical applications. In clinical practice, obese or arm-down patients, and unexpected artifacts may result in increased image noise and decreased SNR and contrast. In this case, understanding the difference in image quality change based on the DLIR intensity makes it possible to obtain accurate images. Several studies have evaluated low-contrast detectability by quantifying contrast-to-noise ratio (CNR) and standard deviation for noise [18, 19]. However, this methodology can be misleading as it neglects factors such as region size, contrast, and image texture [20, 21]. In this study, we used blind-quality-based evaluation parameters, namely NIQE and BRISQUE, to demonstrate their practical applicability in assessing DLIR intensity in the field of imaging. The purpose of this study was to evaluate image quality based on the characteristics of DLIR intensity in abdominopelvic CT using noise level and blind quality evaluations.

2. Materials and Methods

2.1. Phantom and patient selection

This study used an adult male phantom (CIRS, Virginia, USA) and a 256-slice multidetector CT scanner (Revolution; GE Healthcare, Milwaukee, Wisconsin, USA).

This study included 30 consecutive adult patients (10 women, 20 men; mean age \pm standard deviation (SD),

60.26 ± 12.65 years old and mean body mass index of 23.59 ± 3.78 kg/m² (range, 16.18-31.87 kg/m²)) who underwent contrast-enhanced abdominopelvic CT examinations including hepatic venous phase (HVP) CT, between 2015 and 2022. Three patients were underweight, 18 were healthy weight, eight were overweight, and one was obese. All patients underwent CT for clinically indicated reasons. The clinical indications for CT were cancer, liver cysts, chronic liver disease, abdominal pain, sigmoid colon tumor, GB stones, and renal cysts.

The study was conducted according to the guidelines of the Declaration of Helsinki and approved by the Institutional Review Board of Severance Hospital (4-2022-0356).

2.2. CT scanning methods

The phantom scan parameters were as follows: 100 kV, 450 mA average tube current, 0.5 seconds rotation time, and 0.99 pitch. Raw data were reconstructed using DLIR (TrueFidelity, GE Healthcare, Chicago, Illinois, USA) at low-, medium-, and high-strength levels (DLIR-L, DLIR-M, and DLIR-H, respectively) with a 3-mm slice thickness and 0 % overlap.

All abdominopelvic CT scans ranged from 1 cm superior to the diaphragm to the lesser trochanter. HVP CT was obtained 55 s after the attenuation in the abdominal aorta increased to 100 Hounsfield units compared to that at the baseline. When HVP phase images were obtained, an intravenous injection of 2.0 mL/kg (up to a maximum of 150 mL when patients weighed more than 75 kg) of iodinated contrast media (Omnipaque 300 (Iohexol), GE Healthcare, Cork, Ireland) was administered, followed by a bolus injection of 40 mL of saline chaser. The patient scan parameters were as follows: 100 kV, 323 mA average tube current, 0.5-s rotation time, and 0.99 pitch. Raw data were reconstructed using DLIR at medium and high-strength levels (DLIR-M and DLIR-H, respectively) with a 3-mm slice thickness and 0 % overlap.

2.3. Quantitative evaluation of image quality

This study used the COV and CNR parameters as quantitative evaluation methods for assessing the noise levels in CT images. The regions of interest (ROI) for calculating the COV and CNR used in the phantom and patient studies are shown in Fig. 1(a) and Fig. 2(a), respectively. The formulas for calculating COV and CNR are as follows:

$$COV = \frac{\sigma_T}{S_T} \quad (1)$$

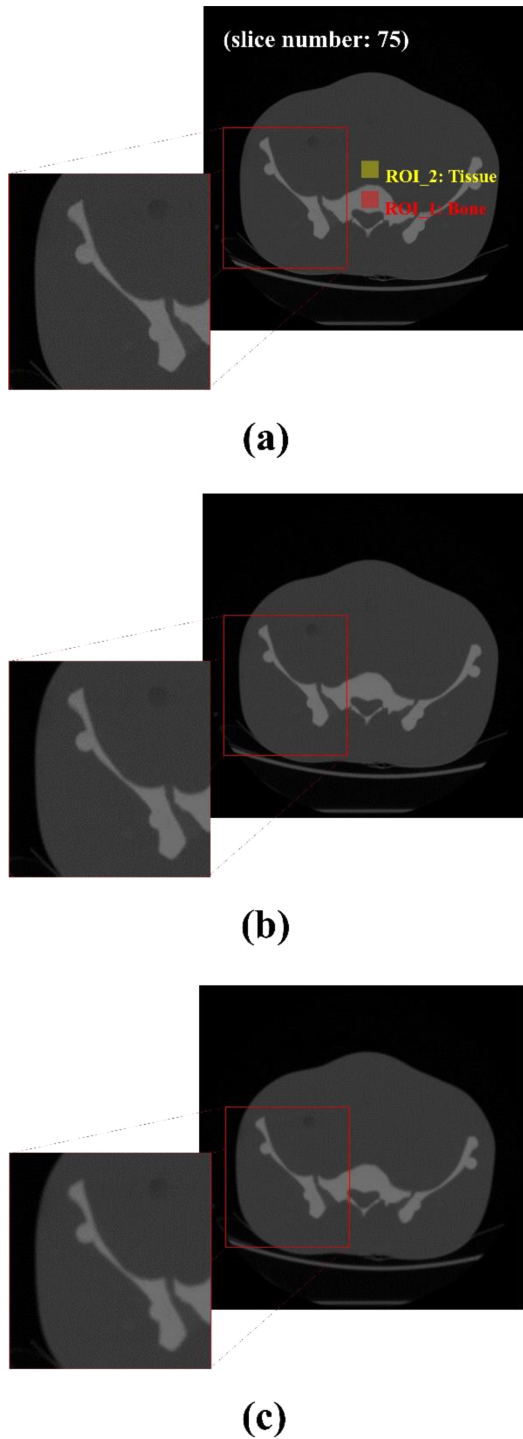


Fig. 1. CT phantom axial images after the application of a deep-learning-based reconstruction algorithm with various intensities: (a) DLIR-L, (b) DLIR-M, and (c) DLIR-H. (a) includes ROIs of the bone and tissue regions for COV and CNR measurements.

$$CNR = \frac{|S_T - S_B|}{\sqrt{\sigma_T^2 + \sigma_B^2}} \quad (2)$$

where S_T and σ_T are the mean and standard deviation values of the target region (bone and tissue), respectively, and are the mean and standard deviation values of the background (ROI_3 in Fig. 2(a)), respectively. Two representative methods were used as blind quality evaluation parameters: natural image quality evaluation (NIQE) and blind/referenceless image spatial quality evaluation (BRISQUE). NIQE and BRISQUE, which can evaluate image quality based on no reference, were introduced by Mittal *et al.* [22, 23]. Both evaluation methods use the principle of including the statistical properties hidden in a natural image through mean subtraction and contrast normalization (MSCN) pre-processing.

3. Results

Fig. 1 shows the resulting image using various deep-learning-based reconstruction algorithms when acquiring a CT phantom image of the 75th slice. A CT image slice in which the bone and tissue regions of the abdomen of the human body were well-marked was selected, and DLIR-L, M, and H were applied to display the image. Fig. 2 shows an image of the result obtained using a deep-learning-based reconstruction algorithm that can be applied when acquiring a real patient's abdominal CT image. Figs. 2(a) and (b) show the abdominal CT images of a real patient obtained by applying DLIR-M and H, respectively. We set such that the middle abdomen, liver, and pelvic areas could be included when selecting the slices for the two images.

To analyze the CT phantom image quantitatively, the noise level and blind quality were evaluated using the ROIs shown in Fig. 1, and the resulting graph is shown in Fig. 3. The COV and CNR results of the CT phantom images obtained using the intensity of the deep-learning-based reconstruction algorithm are shown in Figs. 3(a) and (b), respectively. When DLIR-L, M, and H were applied, the quantitative analysis of COV in the bone region revealed values of 0.0145, 0.0122, and 0.0118, respectively. The COV values in the addition and tissue regions were 0.0178, 0.0148, and 0.0109, respectively, when DLIR-L, M, and H were applied. In CNR values where contrast and noise could be observed simultaneously, values of 55.19, 63.55, and 75.79 were derived from the CT phantom images obtained by applying DLIR-L, M, and H, respectively. We obtained the lowest value in DLIR-L and the most improved value in DLIR-H among the parameters that can evaluate the two noise levels. The NIQE and BRISQUE results of the CT phantom images obtained using the intensity of the deep-

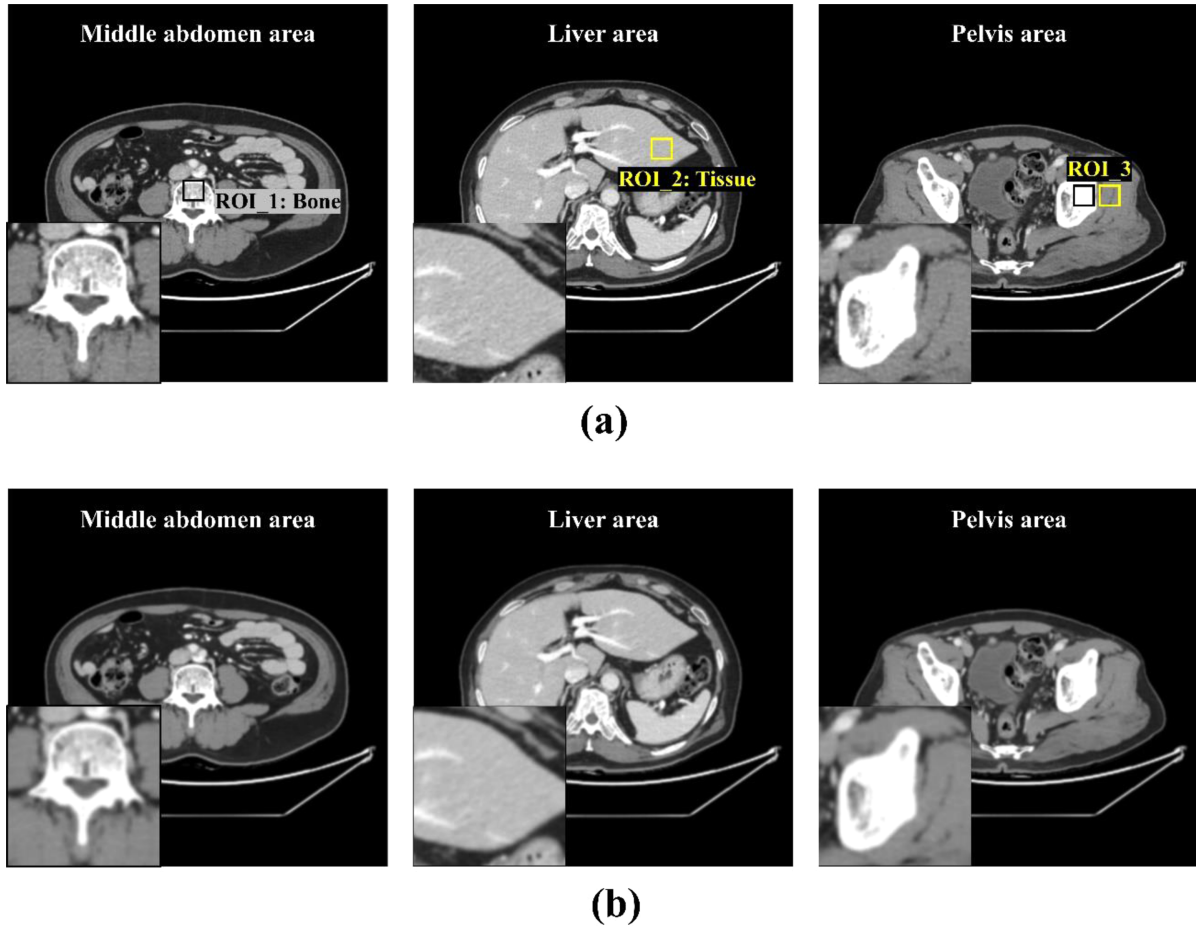


Fig. 2. CT patient axial images after the application of a deep-learning-based reconstruction algorithm with (a) DLIR-M and (b) DLIR-H. The middle abdomen, liver, and pelvis areas were used for CT image evaluation, and ROI_1 and ROI_2 shown in (a) denote COV evaluation, and ROI_3 denotes CNR evaluation.

learning-based reconstruction algorithm are shown in Figs. 3(c) and (d), respectively. Quantitative analysis of the NIQE in the acquired CT phantom images revealed that when DLIR-L, M, and H were applied, the measured values were 8.60, 8.42, and 8.15, respectively. In the case of BRISQUE, values of 42.33, 42.05, and 42.03 were derived from CT phantom images obtained by applying DLIR-L, M, and H, respectively. The NIQE and BRISQUE parameters, which can evaluate blind quality, represent the ideal image quality as the values are smaller, so we could confirm the same trend as the noise level evaluation results.

Results from the CT images of real patients were derived from the average data of all 30 patients. The COV and CNR results of the real patient CT images obtained using the intensity of the deep-learning-based reconstruction algorithm are shown in Figs. 4(a) and (b), respectively. When DLIR-M and DLIR-H were applied during CT image acquisition, the average COV values in

the bone region were 0.0156 and 0.0115, respectively. Furthermore, when DLIR-M and H were applied to acquire the CT images, the average COV values in the tissue area were 0.0191 and 0.0161, respectively. On analyzing the average noise level of CT images of 30 patients, we confirmed that DLIR-H improved COV in the bone and tissue regions by 1.36 and 1.19 times, respectively, compared to DLIR-M. Additionally, we demonstrated that the average CNR was improved by 1.19 times in DLIR-H compared to DLIR-M. The NIQE and BRISQUE results of real patient CT images obtained using the intensity of the deep-learning-based reconstruction algorithm are shown in Figs. 4(c) and (d), respectively. When DLIR-M and H were applied, the quantitative analysis of the average NIQE in the acquired real patient CT images revealed values of 15.17 and 14.33, respectively. Average BRISQUE values of 47.85 and 45.99 were derived from real patient CT images obtained by applying DLIR-M and H, respectively.

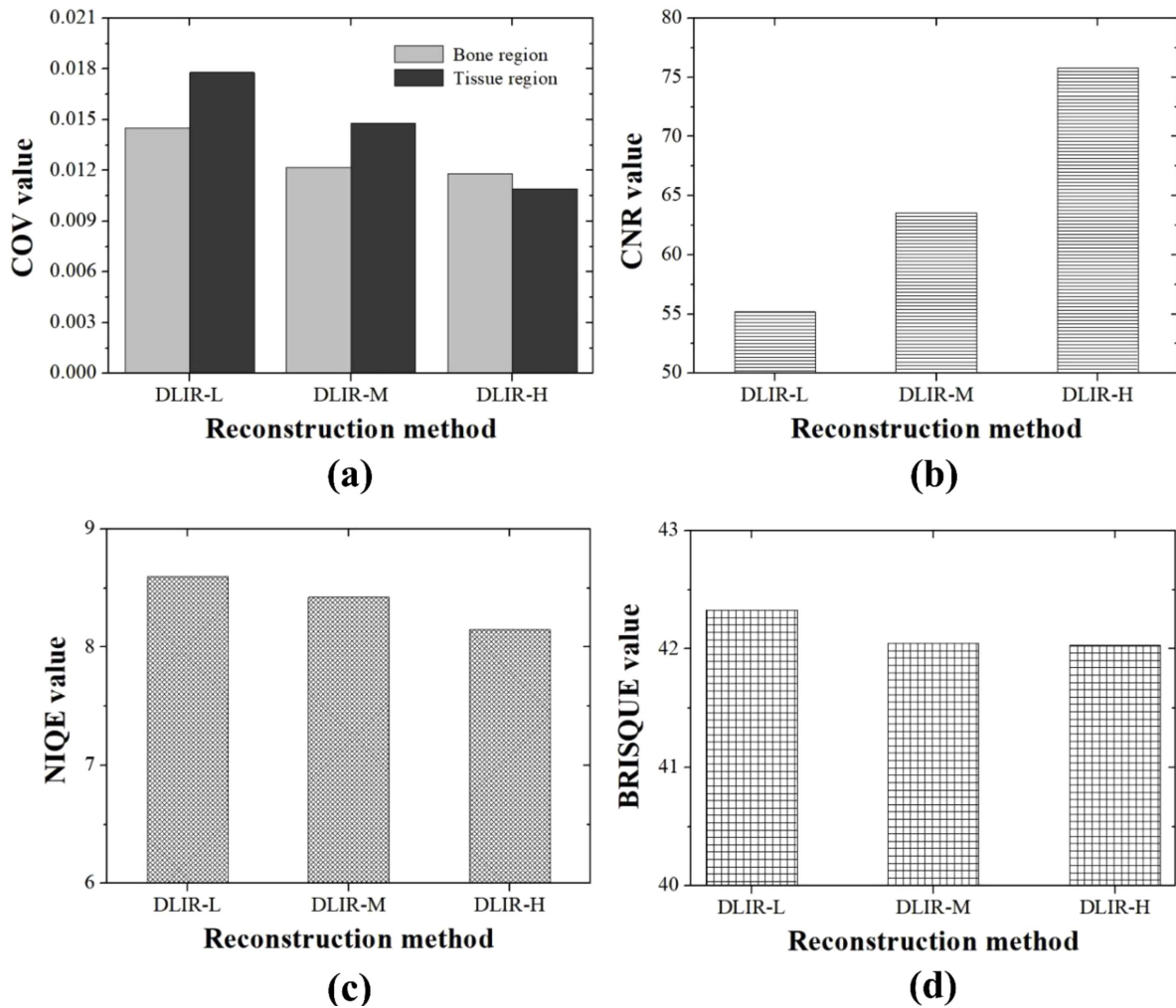


Fig. 3. Graphs of noise level and blind quality evaluation in CT phantom images according to deep-learning-based reconstruction method: (a) COV, (b) CNR, (c) NIQE, and (d) BRISQUE.

4. Discussion

Although IR images were able to reduce the radiation dose while maintaining image quality, it is recommended to use IR of less intensity despite more noise reduction due to unnatural image texture when using IR of strong intensity. The DLIR images trained from the FBP image are expected to have less artificial texture. The design process for a deep learning image reconstruction engine involves creating a Deep Neural Network (DNN) capable of handling millions of parameters. During the training phase, a low dose sinogram is inputted through the DNN and compared to a high dose version of the same data across multiple parameters, such as image noise and low contrast resolution. The network reports the differences via backpropagation and adjusts the strength of the equations until the output image matches the ground truth

image. In the verification phase, the network reconstructs unseen clinical and phantom cases, including rare ones, to confirm its robustness. The Deep Learning Image Reconstruction (DLIR) offers three levels of reconstruction strength (low, medium, high) to control noise reduction. These levels can be incorporated into the reconstruction protocols based on clinical applications and radiologist preference without affecting the reconstruction speed [24]. In this study, a blind quality evaluation parameter that enables image evaluation without a comparison group and a gold standard image were used for image evaluation according to the increase in DLIR intensity. Some studies have evaluated low-contrast detectability by measuring simple CNR and standard deviation for noise [18, 19]. However, this can provide misleading results because the region size, contrast, and image texture are not considered [20, 21]. The blind-quality-based NIQE

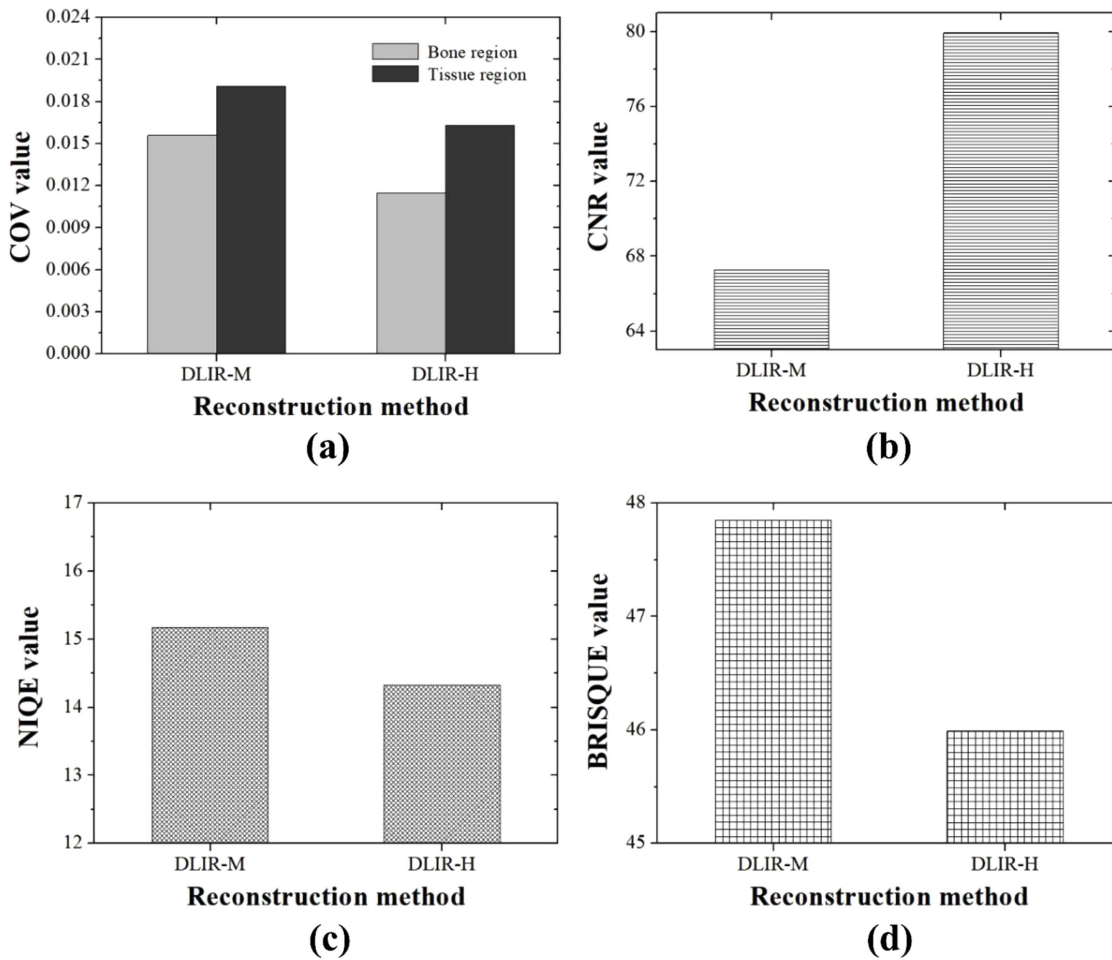


Fig. 4. Graphs of noise level and blind quality evaluation in CT patient images according to deep-learning-based reconstruction method: (a) NIQE results according to DLIR intensity, (b) BRISQUE results according to DLIR intensity; there is a statistically significant difference between DLIR-M and DLIR-H ($p=0.021$), (c) COV (in bone and tissue) results according to DLIR intensity; there is a statistically significant difference between DLIR-M and DLIR-H ($p=0.049$), and (d) CNR results according to DLIR intensity; there is a statistically significant difference between DLIR-M and DLIR-H ($p=0.000$).

and BRISQUE evaluation parameters are well-demonstrated in the field of imaging, enabling the evaluation of clinical utility according to the DLIR intensity. The reason for using NIQE and BRISQUE evaluation factors in this study is to understand the effect of each intensity image without reference and to determine the image intensity more efficiently in clinical practice. This is necessary because iterative reconstruction images and deep-learning-based images have been clinically proven to be superior to FBP images over a long period of time. As a result, the number of tests that perform diagnostic evaluation using repetitive reconstructed images without FBP images is increasing. Therefore, we presented an elaborate analysis of the influence of bone and tissue on the resulting images to help determine DLIR intensity without FBP imaging in clinical practice.

In the phantom study, COV and CNR evaluation resulted in improved noise levels, while the blind quality evaluation of NIQE and BRISQUE resulted in improved values as the reconstruction strength of the DLIR increased. The COV and CNR results showed that when DLIR-H was used, it was improved by approximately 29 % and 37 %, respectively, compared to DLIR-L. Moreover, the results of NIQE and BRISQUE improved by approximately 5 % and 1 %, respectively, when DLIR-H was applied. Consequently, the tendency between the noise level and blind quality evaluation was almost consistent, and noise contributed significantly to the image quality of the overall CT image. The difference in the results for each intensity in the blind quality evaluation was not large (a difference of within 5 %). Based on a previous phantom study, advanced modeled

IR (ADMIRE) showed a greater blind quality evaluation difference than that of DLIR as the intensity increased. Despite the greater noise reduction in ADMIRE 5 than in ADMIRE 3, the more recommended use of ADMIRE 3 in clinical practice is because a stronger ADMIRE intensity results in greater negative image textures, such as plastic and oil paint. Unlike this, DLIR does not have a large intensity-dependent gap in blind quality evaluation. In the case of DLIR, even if noise reduction increases using a strong intensity, it does not increase the artificial image texture.

Jensen *et al.* [25] reported greater diagnostic confidence in DLIR-H and DLIR-M than in DLIR-L. In another study, DLIR-L was not beneficial in terms of noise reduction when compared to IR [26]. In this study, DLIR-M and DLIR-H were analyzed in-depth in the patient study. In the patient study, noise levels through COV and CNR evaluation factors and blind quality evaluation of NIQE and BRISQUE resulted in improved values as the reconstruction strength of the DLIR increased. The COV and CNR results showed that when DLIR-H was used, it was improved by approximately 20 % and 19 %, respectively, compared to that associated with the use of DLIR-M. Further, the results of NIQE and BRISQUE improved by approximately 6 % and 4 %, respectively, when DLIR-H was applied. As with the phantom results, the tendency between the noise levels and blind quality evaluation has been almost consistent. Furthermore, the difference between DLIR-H and DLIR-M in patient images was greater in all evaluations except COV (tissue) than the corresponding differences in the phantom results.

The COV in bones and tissues was ascertained; resultantly, higher reconstruction strength of DLIR in the bone region was associated with a lower COV. Moreover, the lowest COV was observed when DLIR-H was used. Similarly, in the case of the tissue region, a higher reconstruction strength of the DLIR in the bone region was associated with a lower COV. Further, the lowest COV was observed when DLIR-H was used. In the phantom study, the COV, according to the difference in reconstruction strength of DLIR in tissues, exhibited a significant gap compared to that in bones. In patients, there was a significant gap in the COV according to the difference in reconstruction strength of DLIR in both bones and tissues.

In the reconstruction process, the blur of the image edge hinders detection, particularly for small lesions. As reported in previous studies [27], the DLIR-H image was disadvantageous in detecting small malignant lesions and low contrast differences in the hepatic region due to edge blurring. Still, the results of this study were different. In

this study, blurring was only evaluated with the reader's eyes. In this study, the results of BRISQUE were lower at DLIR-H than at DLIR-M, and DLIR-H showed the best performance in terms of the spatial resolution of the image. According to Frank *et al.* [26], low-contrast visibility was the best in DLIR-H due to analyzing the three readers' phantom images, indicating a similar tendency to our results. Another study demonstrated the advantage of DLIR-H for diagnosing small lesions in low-dose abdominal images [28, 29].

This study had several limitations. First, the sample size was relatively small, and the study was conducted at a single hospital, which might have caused selection bias. Second, we used only a single reconstruction kernel. The image texture and edge expression differ depending on the kernel type and when applying DLIR. Third, only one DLIR image acquired from one vendor was evaluated in this study. Thirdly, it is important to note that the evaluation was conducted solely on a commercial deep learning reconstruction package provided by a single vendor. Therefore, further clinical studies are required for devices from other vendors.

5. Conclusion

In this study, abdominal CT image quality was quantitatively evaluated by performing noise level and blind quality evaluations to determine the characteristics according to interpretations in DLIR intensity. The CT image quality improved as the DLIR intensity increased, and the deviation gap based on the DLIR intensity was not large. This study is expected to provide basic research data on the characteristics of DLIR intensity in abdominopelvic CT imaging.

Acknowledgement

This work was supported by the National Research Foundation of Korea (NRF) grant funded by the Korea government (MSIT) (No. RS-2023-00211810) and this work was supported by the Gachon University research fund of 2023 (GCU-202303880001).

References

- [1] L. L. Geyer, U. J. Schoepf, F. G. Meinel, J. W. Nance, G. Bastarrika, J. A. Leipsic, N. S. Paul, M. Rengo, A. Laghi, and C. N. De Cecco, *Radiology* **276**, 339 (2015).
- [2] A. C. Silva, H. J. Lawder, A. Hara, J. Kujak, and W. Pavlicek, *Am. J. Roentgenol.* **194**, 191 (2010).
- [3] J. Leipsic, G. Nguyen, J. Brown, D. Sin, and J. R. Mayo,

- Am. J. Roentgenol. **195**, 1095 (2010).
- [4] K. Lim, H. Kwon, J. Cho, J. Oh, S. Yoon, M. Kang, D. Ha, J. Lee, and E. Kang, *J. Comput. Assist. Tomogr.* **39**, 443 (2015).
- [5] S. Lee, H. Kwon, and J. Cho, *Acad. Radiol.* **23**, 1532 (2016).
- [6] A. Sodickson, P. F. Baeyens, K. P. Andriole, L. M. Prevedello, R. D. Nawfel, R. Hanson, and R. Khorasani, *Radiology* **251**, 175 (2009).
- [7] P. De Marco and D. Origgi, *J. Appl. Clin. Med. Phys.* **19**, 275 (2018).
- [8] H. Kwon, J. Cho, J. Oh, D. Kim, J. Cho, S. Kim, S. Lee, and J. Lee, *Br. J. Radiol.* **88** (2015).
- [9] M. Gatti, F. Marchisio, M. Fronza, O. Rampado, R. Faletti, L. Bergamasco, R. Ropolo, and P. Fonio, *J. Comput. Assist. Tomogr.* **42**, 191 (2018).
- [10] D. Fleischmann and F. E. Boas, *Eur. Radiol.* **21**, 510 (2011).
- [11] Z. Yu, J.-B. Thibault, C. A. Bouman, K. D. Sauer, and J. Hsieh, *IEEE Trans. Image Process.* **20**, 161 (2011).
- [12] Z. Deák, J. M. Grimm, M. Treitl, L. L. Geyer, U. Linsenmaier, M. Körner, M.F. Reiser, and S. Wirth, *Radiology* **266**, 197 (2013).
- [13] N. K. Lee, S. Kim, S. B. Hong, T. U. Kim, H. Ryu, J. W. Lee, and J. Y. Kim, *Am. J. Roentgenol.* **213**, 659 (2019).
- [14] S. Singh, M. K. Kalra, J. Hsieh, P. E. Licato, S. Do, H. H. Pien, and M. A. Blake, *Radiology* **257**, 373 (2010).
- [15] P. Ning, S. Zhu, D. Shi, Y. Guo, and M. Sun, *PLoS One* **9** (2014).
- [16] G. Chartrand, P. M. Cheng, E. Vorontsov, M. Drozdal, S. Turcotte, C. J. Pal, S. Kadoury, and A. Tang, *RadioGraphics* **37**, 2113 (2017).
- [17] A. Mileto, L. S. Guimaraes, C. H. McCollough, J. G. Fletcher, and L. Yu, *Radiology* **293**, 491 (2019).
- [18] S. T. Schindera, D. Odedra, S. A. Raza, T. K. Kim, H.-J. Jang, Z. Szucs-Farkas, and P. Rogalla, *Radiology* **269**, 511 (2013).
- [19] M. E. Baker, F. Dong, A. Primak, N. A. Obuchowski, D. Einstein, N. Gandhi, B. R. Herts, A. Purysko, E. Remer, and N. Vachani, *Am. J. Roentgenol.* **199**, 8 (2012).
- [20] J. Solomon, A. Mileto, J. C. Ramirez-Giraldo, and E. Samei, *Radiology* **275**, 735 (2015).
- [21] F. R. Verdun, D. Racine, J. G. Ott, M. J. Tapiovaara, P. Toroi, F. O. Bochud, W. J. H. Veldkamp, A. Schegerer, R. W. Bouwman, I. H. Giron, N. W. Marshall, and S. Edyvean, *Phys. Med.* **31**, 823 (2015).
- [22] A. Mittal, A. K. Moorthy, and A. C. Bovik, *IEEE Trans. Image Process.* **21**, 4695 (2012).
- [23] A. Mittal, R. Soundararajan, and A. C. Bovik, *IEEE Signal. Process. Lett.* **20**, 209 (2013).
- [24] J. Hsieh, E. Liu, B. Nett, J. Tang, J.-B. Thibault, and S. Sahney, GE Healthcare: Chicago, IL, USA (2019).
- [25] C. T. Jensen, X. Liu, E. P. Tamm, A. G. Chandler, J. Sun, A. C. Morani, S. Javadi, and N. A. Wagner-Bartak, *Am. J. Roentgenol.* **215**, 50 (2020).
- [26] C. Franck, G. Zhang, P. Deak, and F. Zanica, *Phys. Med.* **81**, 86 (2020).
- [27] T. Kaga, Y. Noda, K. Fujimoto, T. Suto, N. Kawai, T. Miyoshi, F. Hyodo, and M. Matsuo, *Clin. Radiol.* **76**, 710.e15 (2021).
- [28] M. Akagi, Y. Nakamura, T. Higaki, K. Narita, Y. Honda, J. Zhou, Z. Yu, N. Akino, and K. Awai, *Eur. Radiol.* **29**, 6163 (2019).
- [29] L.-L. Li, H. Wang, J. Song, J. Shang, X.-Y. Zhao, and B. Liu, *J. Xray. Sci. Technol.* **29**, 361 (2021).